SUPPORTING INFORMATION

Ultra high performance Supercapacitor from Lacey Reduced Graphene Oxide Nanoribbons

Vikrant Sahu, Shashank Shekhar, Raj Kishore Sharma, and Gurmeet Singh**

Department of Chemistry, University of Delhi, Delhi 110 007, India

Author for correspondence:
Phone +91 11 27666616, drrajksharma@yahoo.co.in (Raj K Sharma)
gurmeet123@yahoo.com (G. Singh)

Calculation of specific capacitance from cyclic voltammetry[1]

$$C_{sp} = \int_{E_1}^{E_2} i(E)dE \,/\, 2(E_2 - E_1)\, mv \quad (1)$$

C_{sp}, is the specific capacitance of single electrode in three cell assembly.

E_1 & E_2 , are the cut off potential of cyclic voltammetry.

i(E), instantaneous current

$\int_{E_1}^{E_2} i(E)dE$, integration of positive and negative sweep in cyclic voltammograms to get the total voltammetric charge.

$E_2 - E_1$, width of potential window

m, mass of material on the electrode

v, scan rate potential

Calculation of energy density and power density

The device capacitance (C_m), energy density and power density were calculated from galvanostatic charge discharge (GCD) by using the following equations[2] [2-4]:

$$C_m = \frac{i \, x \, \Delta t}{m \, x \, \Delta V} \quad (2)$$

$$E = \frac{1 \, x \, Cm \, x \, \Delta V^2}{2 \, x \, 3.6} \quad (3)$$

$$P = \frac{3600 \, x \, E}{\Delta t} \quad (4)$$

Where C_m device capacitance F/g, i is current density (A/g), ΔV voltage after IR-drop (V), m mass loading on two electrodes (mg), Δt discharge current(s), E energy density ($Whkg^{-1}$) and P power density (Wkg^{-1}).

Calculation of Areal capacitance

Areal capacitance calculated from GCD according to the following equation[3]:

$$\boldsymbol{C = \frac{I\Delta t}{S\Delta V}} \quad (5)$$

I - discharge current, Δt – discharge time, S – effective electrode area, ΔV – discharge potential window after IR drop.

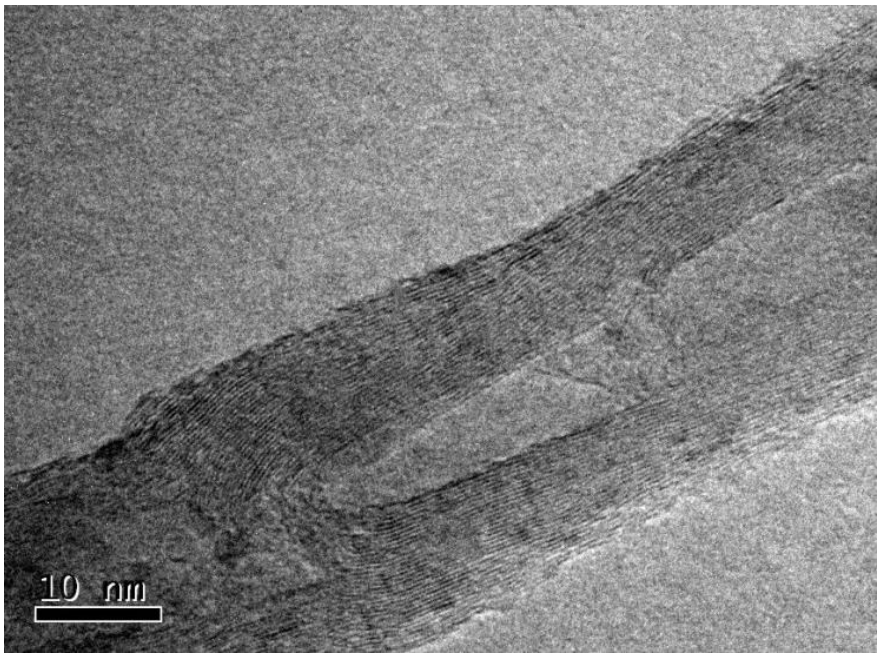

Fig. S-1: High resolution transmission electron micrograph (HRTEM) of MWCNT used for the synthesis of LRGONR. Micrograph shows that the MWCNT is composed of ~ 45 concentric, single walled carbon nanotubes. Thus upon opening in axial direction, a stack of about 40-45 graphene nnaoribbons is expected. The MWCNT (purchased from nanoChina) were approx 2 μm long and the diameter varies from 10-35 nm.

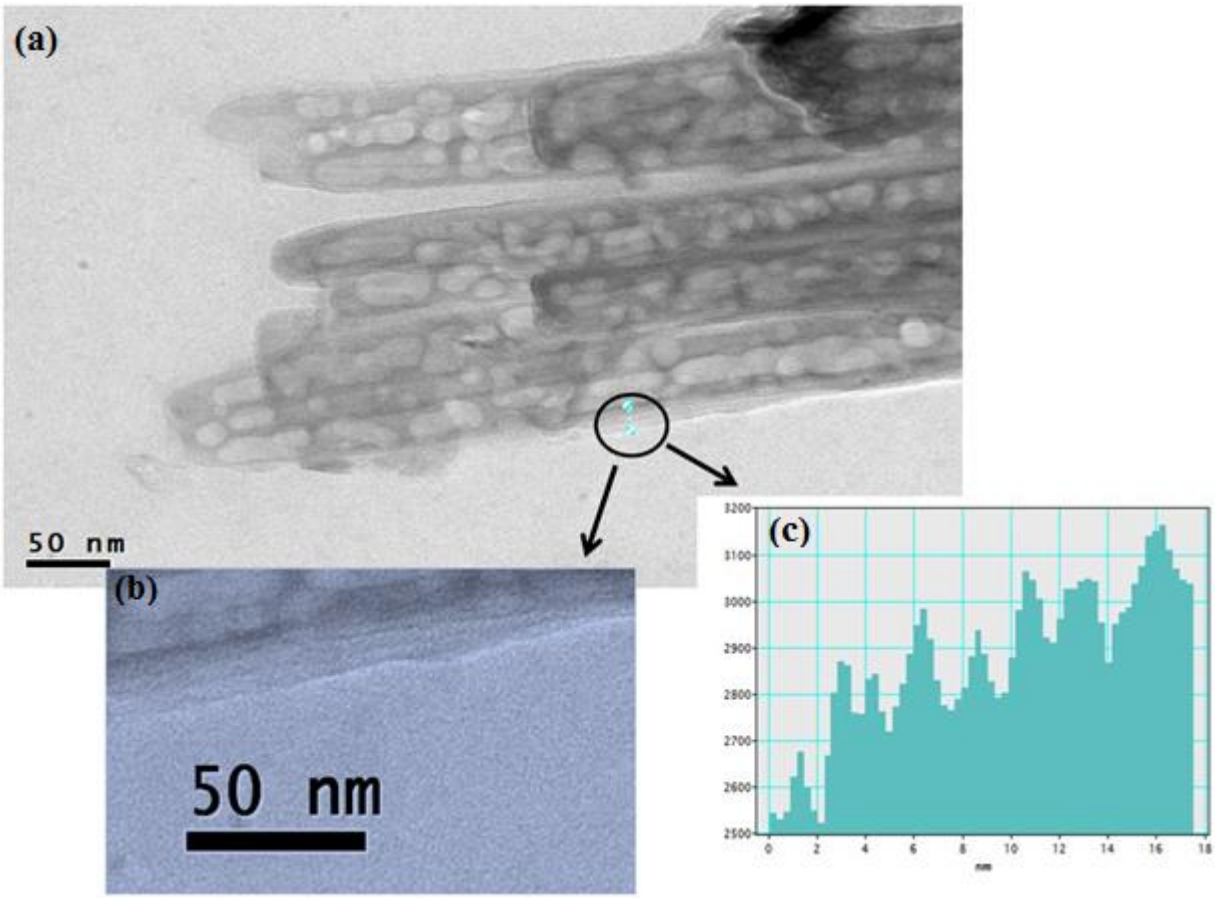

Fig. S-2: (a) Shows entangled LRGONR structures in 2-3 graphene layers stacking. The magnified image (b) show the 4-5 entangled LRGONR and the thickness of this scaffold is estimated to be around 18 nm using Gatan digital micrograph software (image c). The thickness a single LRGONR is estimated ~ 2.0 nm. Oxygen containing functionalities, corrugation and protrusion will add some thickness to each graphene nanoribbon making these around 1 nm thick. The ripples due to protrusion are likely to be <0.5 nm high and 10-50 nm wide. Such a protrusion and some corrugation in the single graphene layer make it ~1.0 nm thick and a single LRGONR (2 layer graphene) as > 2 nm. The thickness (~18 nm) of the stack of ~4 LRGONR is observed due to the corrugation and protrusion in individual ribbon.

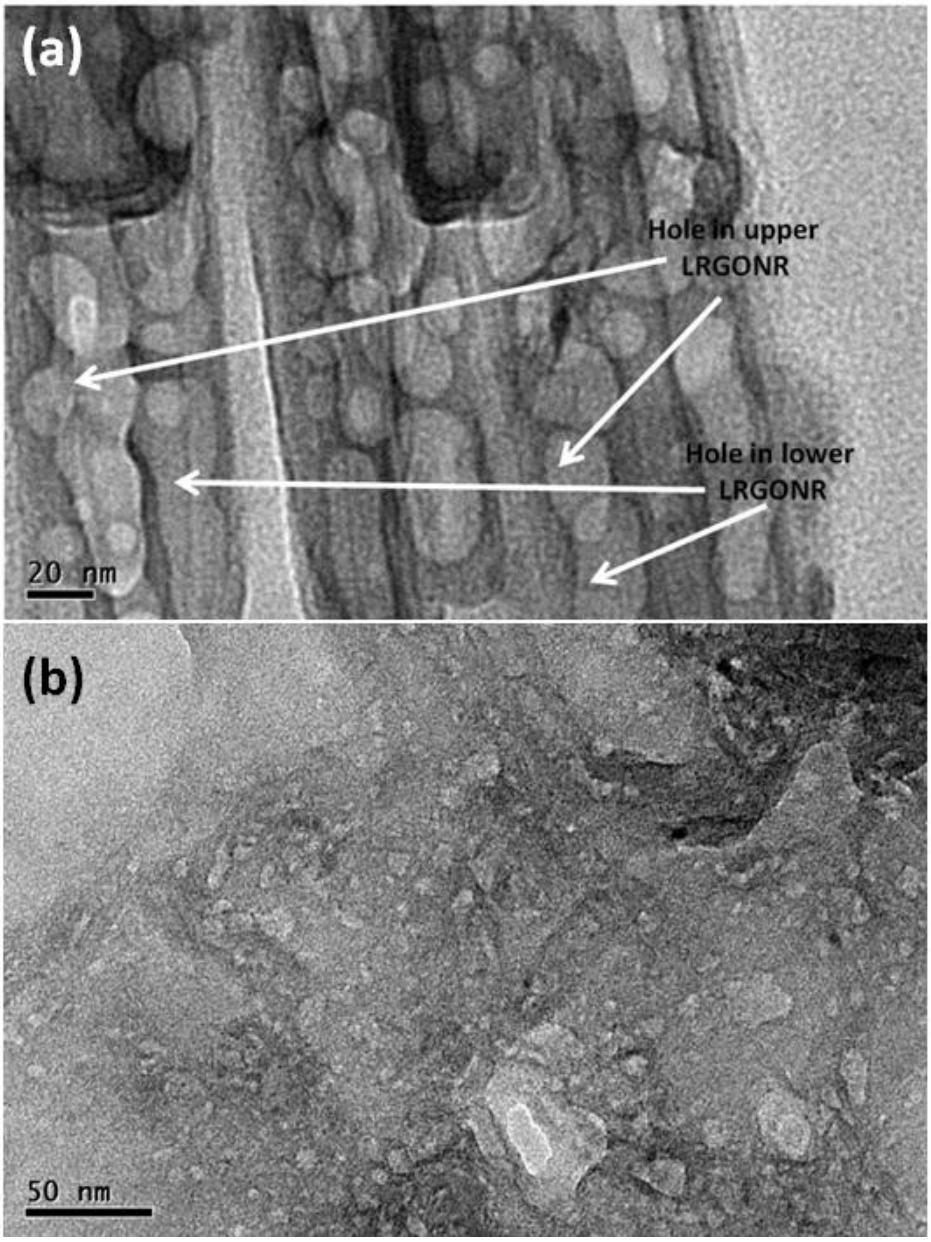

Fig. S-3: (a) Magnified HRTEM image of LRGONR showing 3-4 layer stacking. Image shows that the holes are non co-centric and non centro-symmetric. The reason behind such random hole formation is that after unzipping a nanotube, permanganate (MnO_4^-) moiety due to very small ionic size (~ 0.4 nm) goes between two stacked layers of GONR, attacks at a diene and continues in the vicinity, creating defect. Density and size of such defects/holes depends on the reaction time. Image shows ~3 single layers of lacey graphene ribbon in the form of a LRGONR. Due to the uneven holes distribution van der Waals interactions between two graphene layers are expected to reduce significantly leading to very less stacking and very high electrolytic accessibility. (b) HRTEM image showing the large distribution of LRGONR.

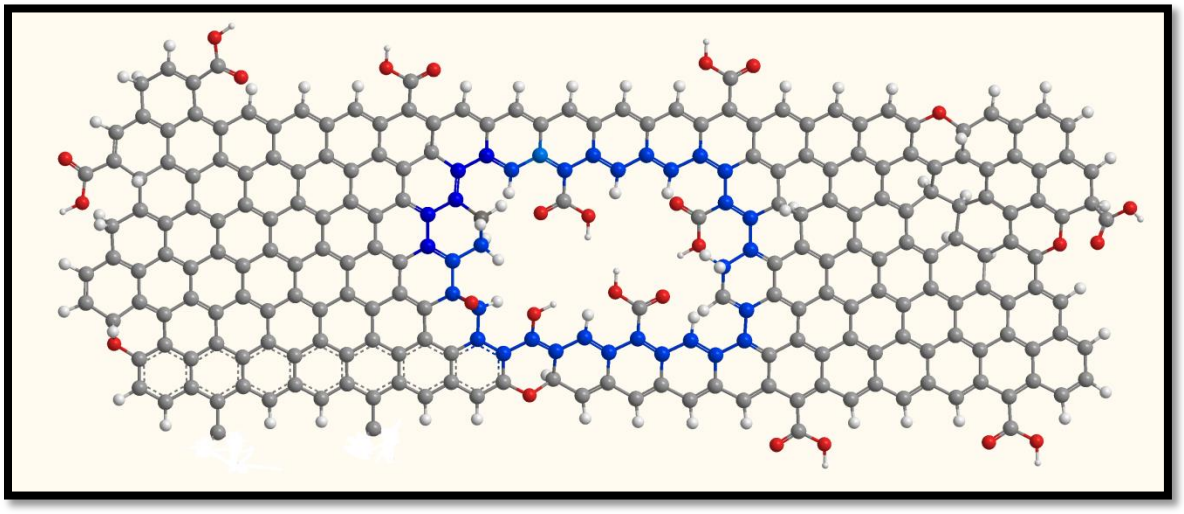

Fig. S-4: Molecular structure of LRGONR.

Due to the high density of states at the edge planes, LRGONR has high tendency to develop electro-active surface groups. Molecular structure of LRGONR is designed according to the carbon/oxygen ratio (~15), obtained from the XPS spectra of LRGONR. The lower part of the ribbon is used to show resonance in sp^2 hybridized carbon of LRGONR which indicate the electronic conduction. As observed in XPS results, ~7 % oxygen is present in the form of carboxylic, epoxy or phenolic surface groups. Edge planes are the highly possible sites for the above surface groups to form through dangling bond. Since sp^2 hybridized carbon is planar geometry and sp^3 carbon is tetrahedral geometry. Therefore, wherever oxygen is forming a bond with the carbon (phenolic or carboxylic), sp^2 carbon of a graphene layer will convert into sp^3 carbon causing hindrance in planar geometry. This gives give rise to protrusion, corrugation in ribbon leading to inter-graphene separation. In LRGONR model image the red color balls demarcate the oxygen; grey as carbon and white balls shows the continued variable length of carbon structure.

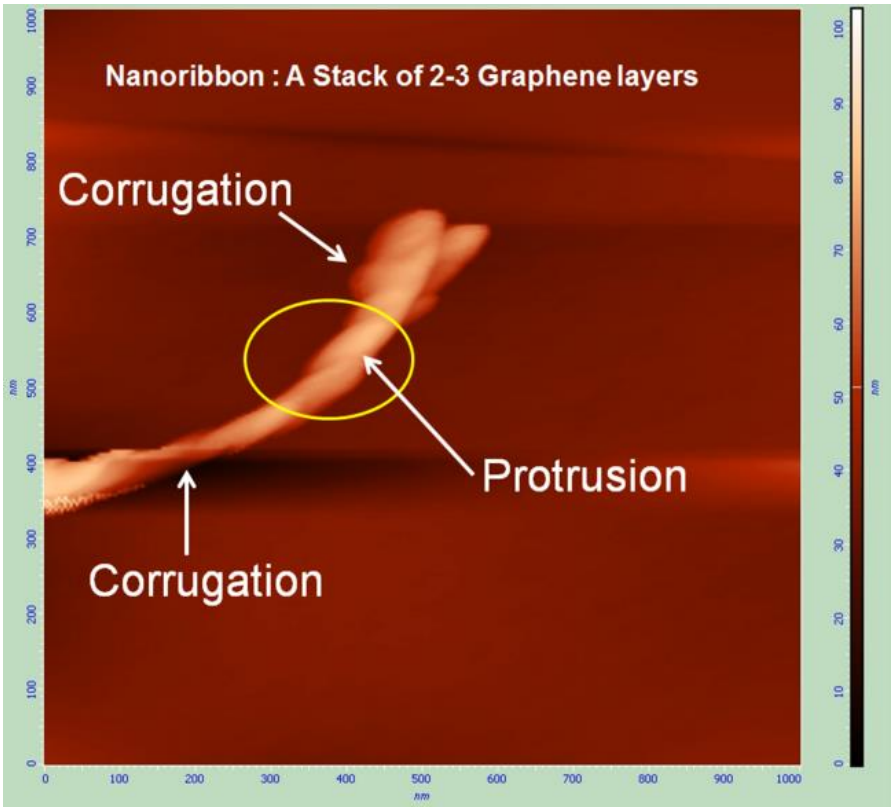

Fig. S-5: AFM image showing protrusion and corrugation in Lacey reduced graphene oxide nano-ribbons

AFM of LRGONR, taken by drop casting an ultra dilute solution of LRGONR over mica sheet in non contact mode using NT-MDT NTEGRA machine is shown in Fig S5. As discussed in Figures (S2-S4) the hole formation increased the density of defects at edge planes and thus the number and location of Sp^3 carbons increased randomly. The oxygen related surface groups attached to Sp3 carbons posses a bond in different angle and thus cause a protrusion at the edge plane (circumference of a hole). Such an arrangement creates space between to entangle graphenes sheets in LRGONR.

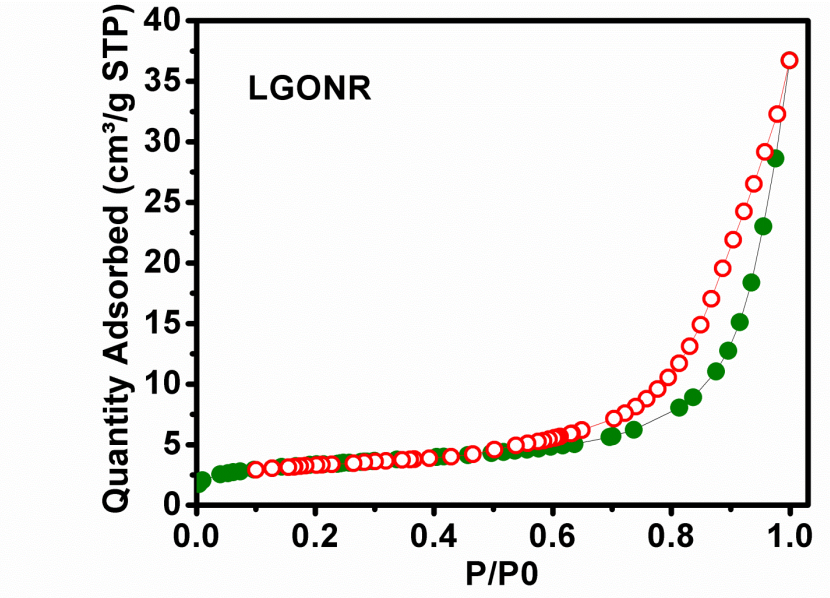

Fig. S-6: N_2 adsorption-desorption isotherm of LGONR.

The hysteresis loop around P/P_0 (0.8 to 1) is nearly parallel to Y-axis which belongs to H1 type curve. This type of loop indicates the presence of secondary mesopores without interconnected channels. This is possible in agglomerated materials and stacked sheets of LGONR.

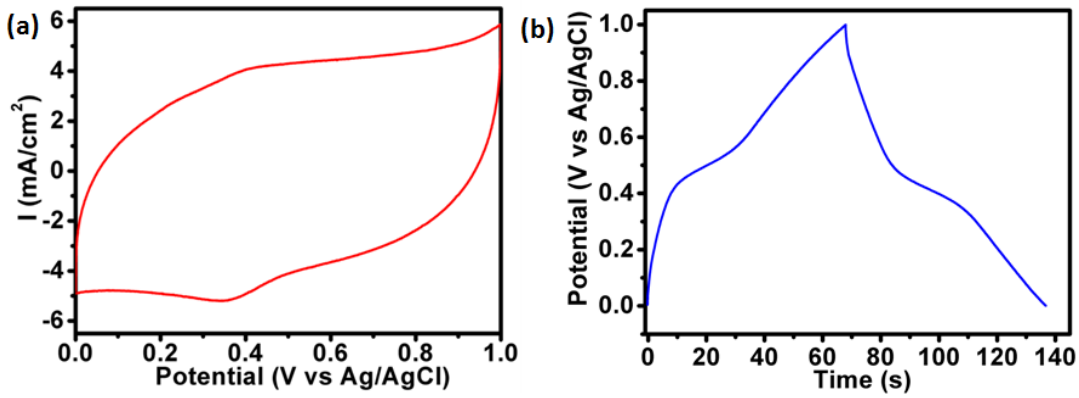

Fig. S-7. (a) CV of LRGONR in 2M H_2SO_4 (in 3 electrode cell) at 5 mV/s, (b) galvanostatic discharge curve (3-electrode cell) of LRGONR at 3 mA.

3 electrode cell galvanostatic charge discharge was carried out in 2M H_2SO_4 to re-confirm the origin of high specific capacitance observed CV measurements with Ag/AgCl reference electrode. Figure S7 (a) depicts a voltammogram of LRGONR recorded at 5 mV/s and the (b) represent the charge discharge characteristics of LRGONR electrode in 3 cell assembly. The loading of LRGONR on 1 cm^2 area was kept constant in both cases to 0.35 mg. The CV (3 cell) specific capacitance at 5 mV/s was found to be 621 F/g (Fig S-7a) and specific capacitance calculated from 3 electrode cell GCD measurement is 604 F/g at 3 mA (Fig S-7 (b), these values are in agreement. The value 3 mA in GCD was chosen because of its closeness to the observed average current in CV (at 5 mV/s)

The charge/discharge curve is found to be non-linear which strongly endorse the involvement of pseudocapacitive contribution at ~4.0 V. The potential, (~0.4V) at which the GCD characteristics take a change in slope is reflected by the pseudocapacitive peaks in voltammogram of Fig. S-7(a). Thus, suggesting that the pseudocapacitance has significant contribution in total charge storage capacity of LRGONR.

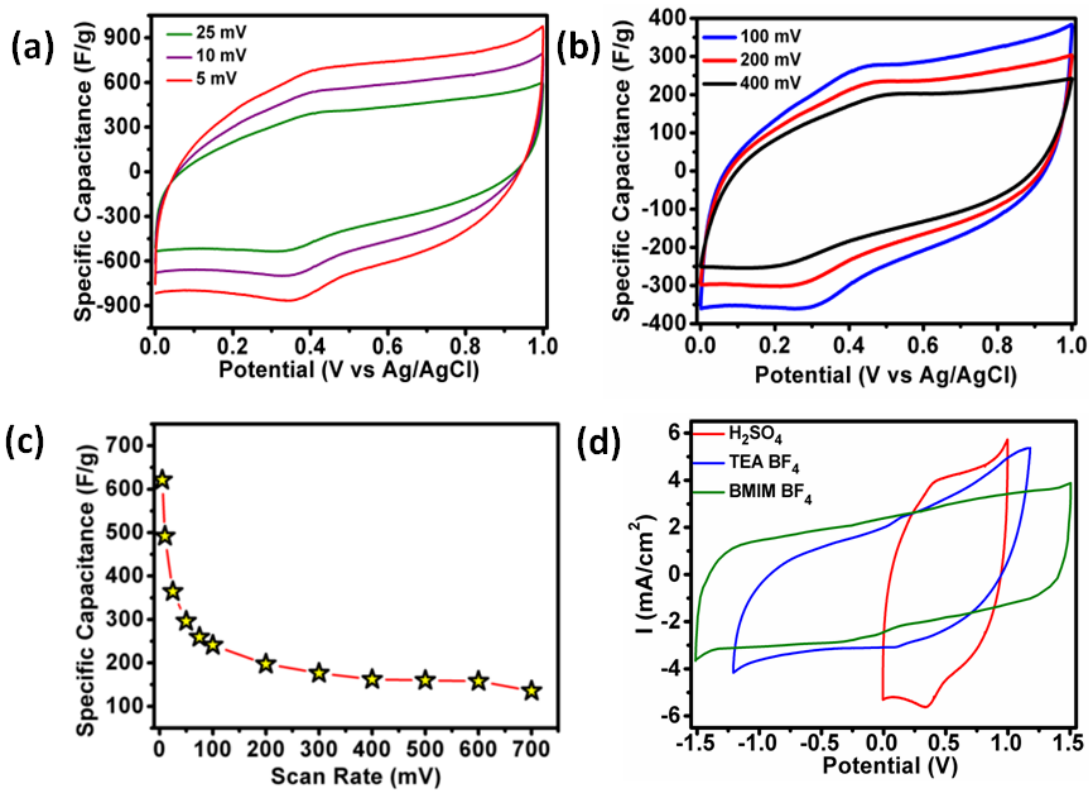

(e) Table:	Areal capacitance or LRGONR supercapacitor at 1mA		
LRGONR in different electrolytes	2.0 M H_2SO_4	1M TEA BF_4/AN	1M BMIM BF_4/AN
Areal Capacitance mF/cm^2	**69.36**	**70.56**	**101.4**

Fig. S-8: (a,b) shows the cyclic voltammograms (CV) of LRGONR electrode at high scan rate and (c) rate capability up to 700 mV/s. (d) CV curve of LRGONR in Current-Voltage scale are shown in Fig. S-8 d. The table (e) presents areal capacitance in different electrolytes using GCD method.

Rate capability of the electrode is related to the rate of charge/discharge which in turn depends on the electrode resistance and the easy accessibility of the electrolytic ions. Figures show (Fig S-8 a,b) shows good establishment of EDL and pseudocapacitive charge storage. Nearly rectangular characteristics at high scan rate (Fig S-8b) implicate the high performance electrode material. Fig S-8c shows the excellent rate capability plot of LRGONR. This clearly demonstrate that even at very fast scan rate, LRGONR electrode store a high figure of charge with good rate capability.

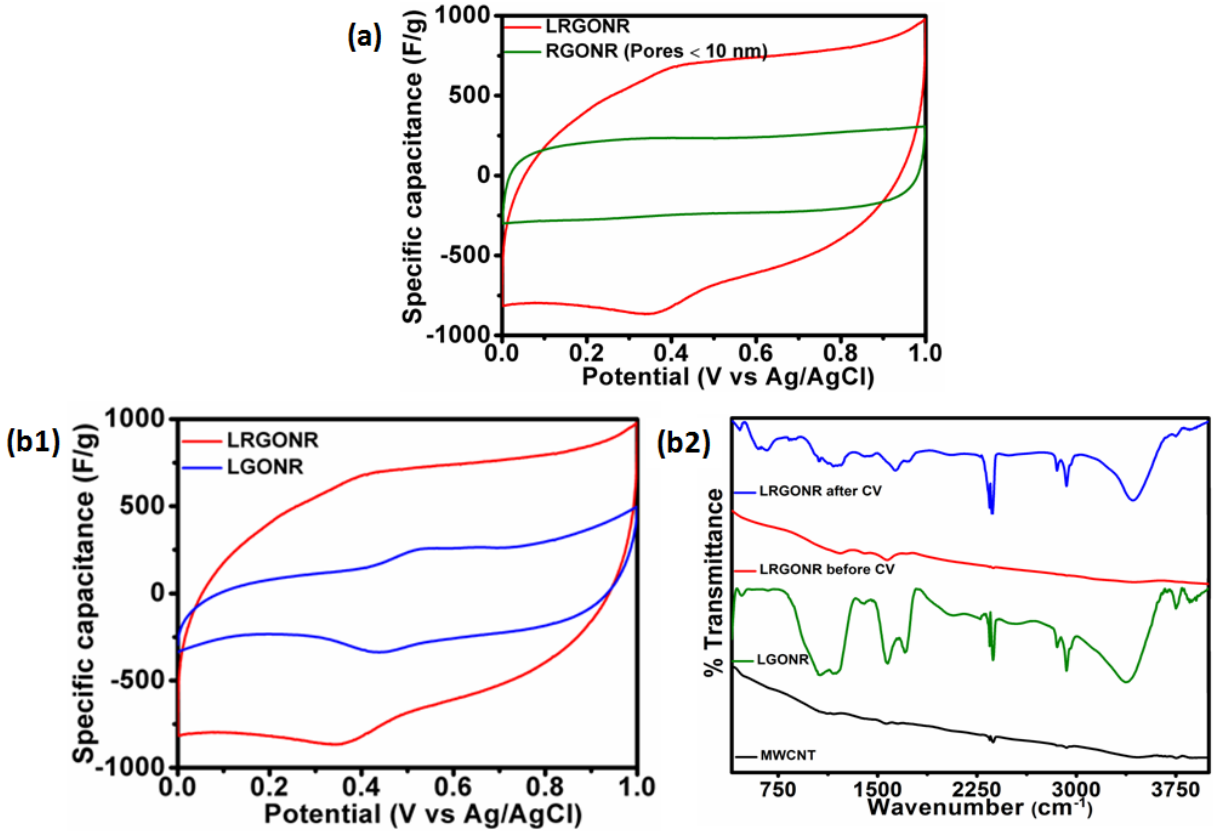

Fig. S-9: (a) Comparative CV of LRGONR and LGONR electrode, (b1) Comparative CV of LRGONR and RGONR (Pores <10 nm) in 2M H_2SO_4, (b2) FTIR spectra of MWCNT, LGONR, LRGONR before CV and LRGONR after few CV cycles.

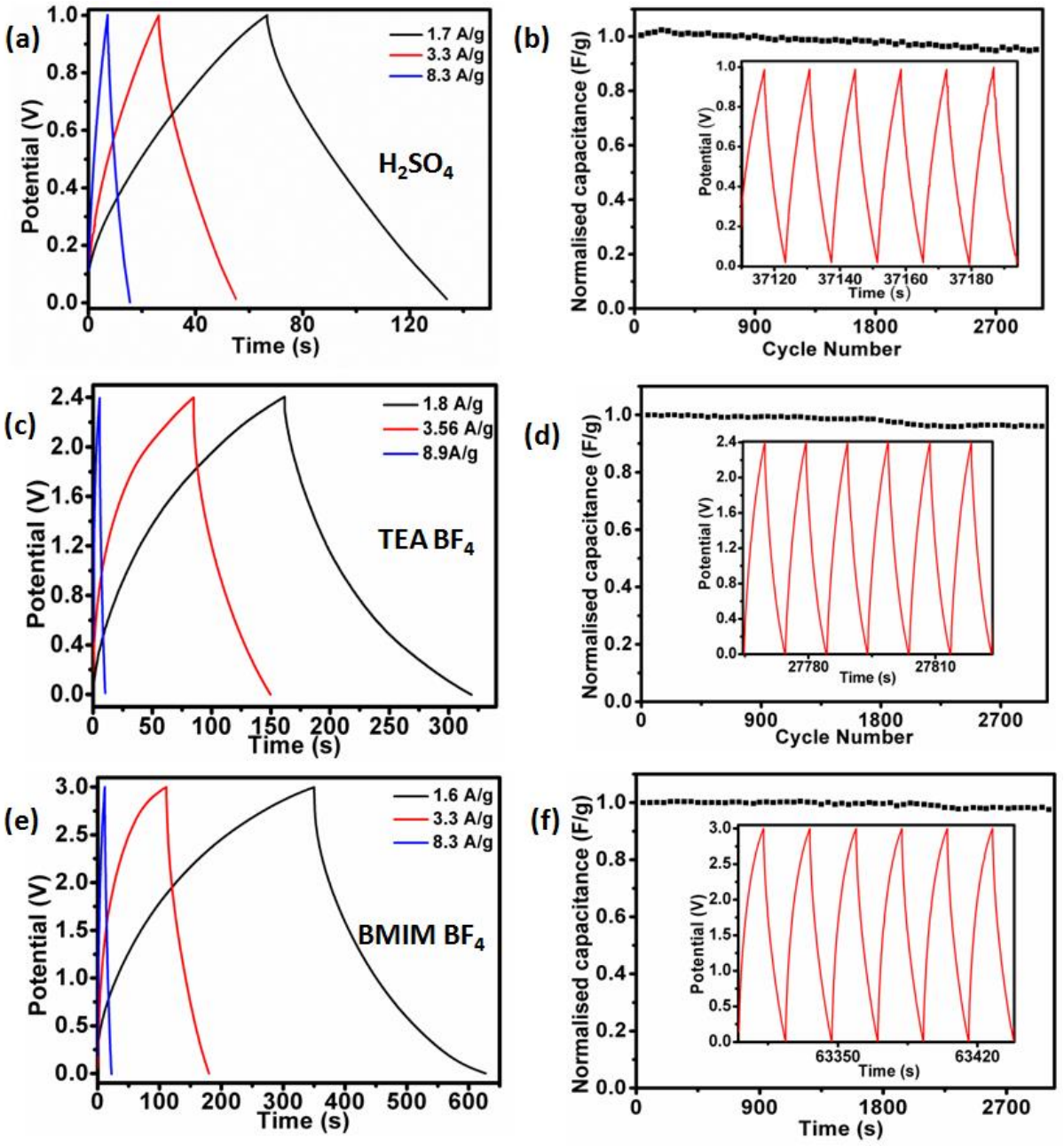

Fig. S-10: LRGONR supercapacitor galvanic charge discharge in 2M H_2SO_4 at 1.7, 3.3 and 8.3 Ag^{-1} (a), organic electrolyte (TEA BF_4) at 1.8, 3.56 and 8.9 Ag^{-1} (c) and ionic electrolyte BMIM BF_4 at 1.6, 3.3 and 8.3 Ag^{-1}(e) respectively. (b,f and d) corrosponding cycling life and capacity retention at high current density 8.3 Ag^{-1} (2M H_2SO_4 and 1M BMIM BF_4) and 8.9 Ag^{-1} (1M TEA BF_4).

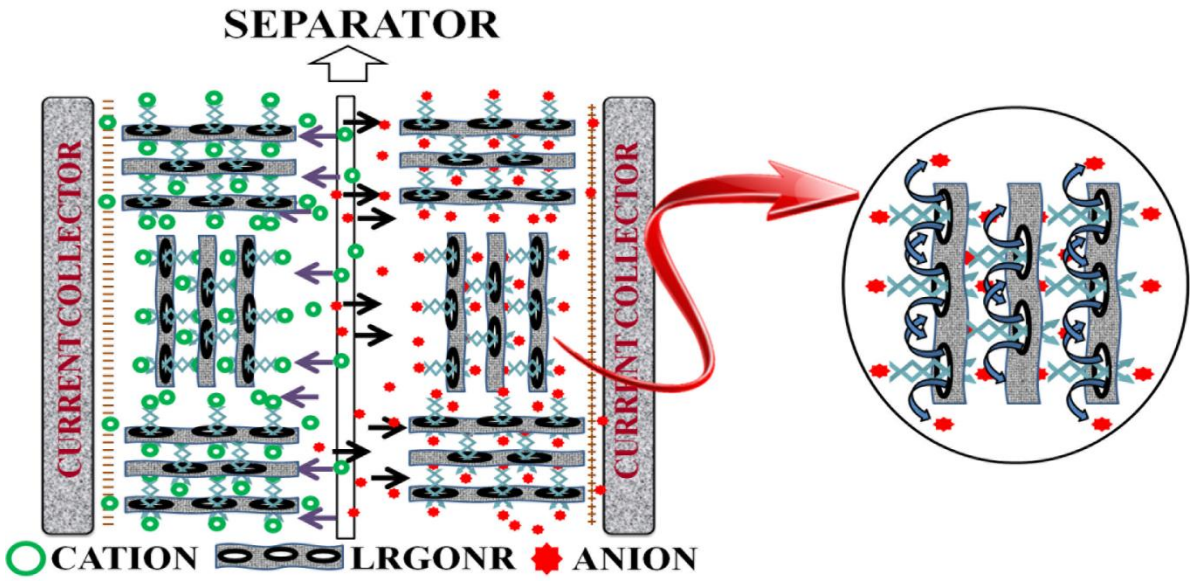

Fig. **S-11:** Schematic of supercapacitor device fabricated by LRGONR represents the pictorial insight view of LRGONR supercapacitor device. Inset depicts the mechanism how the holes in LRGONR efficiently allow the access of electrolyte ions through, and in different layers of graphene nanoribbons resulting in complete utilization of both sides of lacey graphene surface.

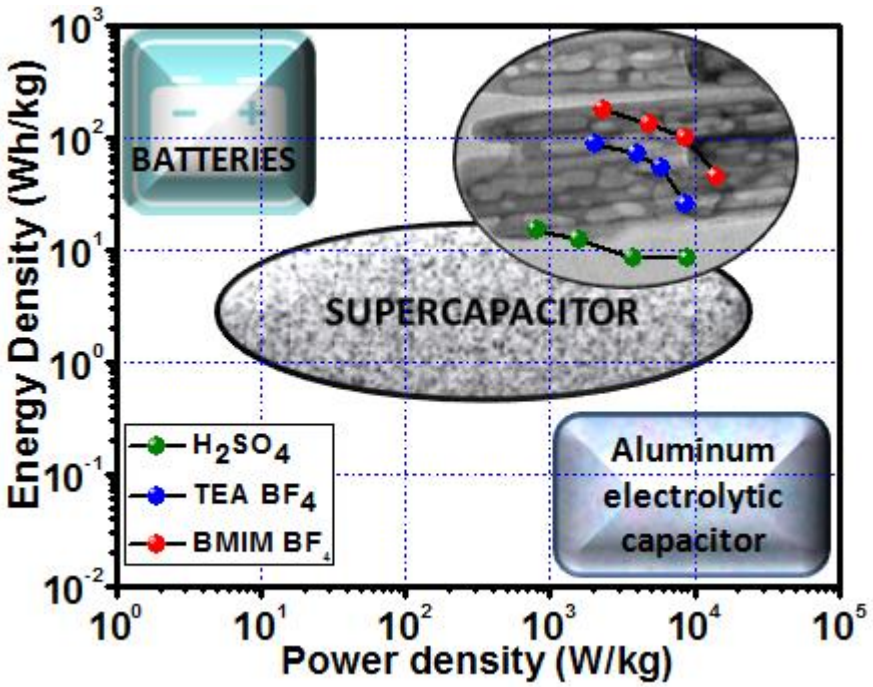

Fig. S-12: Ragone plot of LRGONR depicting the energy and power density in three different different electrolytes.

References

[1] Chen, W.; Fan, Z.; Gu, L.; Bao, X.; Wang, C. Enhanced Capacitance of Manganese Oxide via Confinement Inside Carbon Nanotubes. Chem. Commun. **2010**, *46*, 3905-3907.

[2] Grover, S.; Shekhar, S.; Sharma, R. K.; Singh, G. Multiwalled Carbon Nanotube Supported Polypyrrole Manganese Oxide Composite Supercapacitor Electrode: Role of Manganese Oxide Dispersion in Performance Evolution *Electrochim. Acta* **2014**,116, 137-145.

[3] Yang, P.; Xiao, X.; Li, Y.; Ding, Y.; Qiang, P.; Tan, X.; Mai, W.; Lin, Z.; Wu, W.; Li, T.; Jin, H.; Liu, P.; Zhou, J.; Wong, C. P.; Wang, Z. L. Hydrogenated ZnO Core-Shell Nanocables for Flexible Supercapacitors and Self-Powered Systems. *ACS Nano* **2013**, *7*, 2617–2626.